frontiers | Frontiers in Earth Science

TYPE Original Research
PUBLISHED 10 February 2023
DOI 10.3389/feart.2023.1137157

OPEN ACCESS

EDITED BY
Hossein Azizi,
University of Kurdistan, Iran

REVIEWED BY
Huan Li,
Central South University, China
Dan-Ping Yan,
China University of Geosciences, China

*CORRESPONDENCE
Xu-Jie Shu,
xjshu@ntu.edu.cn

SPECIALTY SECTION
This article was submitted to Petrology, a section of the journal Frontiers in Earth Science

RECEIVED 04 January 2023
ACCEPTED 01 February 2023
PUBLISHED 10 February 2023

CITATION
Shu X-J, Jiang W, Wang D, Cheng C and Wang H-Z (2023), Origin and implication of two newly identified peraluminous A-type granites in the early Paleozoic orogeny, Southeast Asia.
Front. Earth Sci. 11:1137157.
doi: 10.3389/feart.2023.1137157

Origin and implication of two newly identified peraluminous A-type granites in the early Paleozoic orogeny, Southeast Asia

Xu-Jie Shu*, Wei Jiang, Dan Wang, Cheng Cheng and Hong-Zuo Wang

School of Geographic Science, Nantong University, Nantong, China

Abstract: The amalgamation of the Yangtze and the Cathaysia Block in Neoproterozoic time led to the formation of the South China Block (SCB) and generated the Jiangnan Orogen with the occurrences of juvenile magmatic rocks. After this orogeny, a typical collisional orogen formed during the early Paleozoic period in Southeast Asia which is mainly distributed in the Wuyi-Nanling-Yunkai area in the SCB. However, the transitional time from syn-collisional compression to post-collisional extension is debatable. Here, we present new data on zircon U-Pb zircon ages, Lu-Hf isotopes, and geochemistry for the Guzhang and Shadi granites from the Nanling area, South China. Both plutons have similar zircon $^{238}U/^{206}Pb$ ages of ca. 430 Ma. Petrographic and geochemical characteristics (e.g., $FeO^t/(FeO^t+MgO)$ = 0.82–0.95) indicate that both granites are peraluminous A-type, with high Ga/Al ratios (2.43–2.91) as well as high concentrations of Zr, Nb, Ce, Y (sum values from 327 to 527 ppm), and formation temperature (820°C–845°C). Shadi granite exhibit high positive εHf(t) values (clustering within 0 to +6) while Guzhang granite show relatively lower εHf(t) values (–8.7 to –2.9). Their mildly negative to positive zircon εHf(t) values are higher than that of many coeval granites and can be derived from anhydrous melting of tonalitic genesis in the middle crustal depth, with the Shadi pluton having more orthometamorphite in the source. The ages and Hf isotopic compositions of inherited zircons (εHf(t = 960 Ma) = 9.2, εHf(t = 950 Ma) = 7.3) suggest that the Neoproterozoic juvenile magmatic rocks in the Jiangnan Orogen were a significant source for these granites. We interpret these A-type granites derived at the post-collisional stage. Their occurrence indicates that the geological setting of this Paleozoic orogen shifted from compression to extension no later than 430 Ma.

KEYWORDS

orogenic magmatism, A-type granite, early Paleozoic, Southeast Asia, geological setting

1 Introduction

A nearly 2000 km long and 450 km wide orogen formed in Southeast Asia during the Ordovician to Silurian periods (Figure 1; Charvet et al., 2010; Li et al., 2010; Zhao et al., 2022). This collisional belt was characterized by widely distributed regional metamorphic rocks (greenschist, amphibolites, and minor granulites) in the Wuyi-Nanling-Yukai area with ages ranging from 460 to 436 Ma (e.g., Shu et al., 2008; Charvet et al., 2010; Yu et al., 2014). The orogeny also caused angular unconformity between the Devonian and pre-Devonian strata.

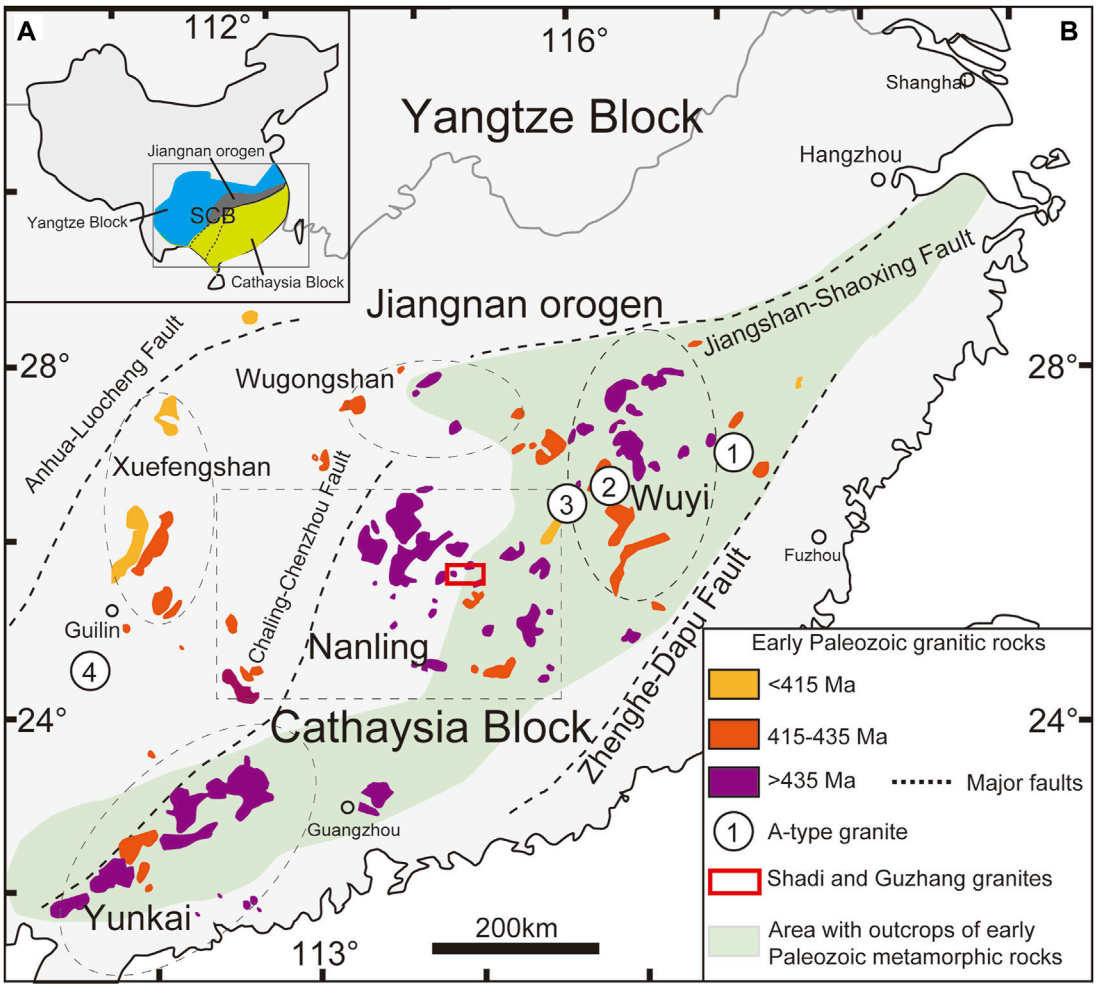

FIGURE 1
Age distribution map of early Paleozoic granitic rocks in South China Block. Most of the metamorphic and magmatic rocks are distributed in the WuYi-Nanling-Yukai area. The A-type granites (marked with ①~④) are uncommon and have ages from 415 to 400 Ma. The Jiangshan-Shaoxing fault is thought to be the boundary between the Yangtze and the Cathaysia block at the Neoproterozoic time while the westward extension of the boundary is unclear(marked as the dotted lines in Figure 1A.

The origin of this early Paleozoic orogen was long timely debated from the early 1990s to the present (e.g., Ren et al., 1997; Lin et al., 2018; Wang et al., 2018). The main point of contention is whether the orogen formed with or without oceanic crust subduction. The lack of early Paleozoic ophiolites, magmatic volcanic rocks, subduction complexes, and high-pressure metamorphism was cited as evidence for intracontinental origin (Charvetet al., 2010; Li et al., 2010; Shu et al., 2014; Wang et al., 2013; Yao et al., 2012; Kong et al., 2021; Zhao et al., 2022). While the oceanic crust subduction model is supported by a few newly discovered arc-like rocks with ages from 445 to 430 Ma (Peng et al., 2006; Peng et al., 2016; Zhang et al., 2016; Lin et al., 2018). To our opinion, the lack of abundant volcanic rocks and detrital zircons with ages ranging from 520 to 460 Ma in the adjacent strata and river sands of South China (Xu et al., 2007) may further support the intra-continent model.

Despite this debate, the geological processes related to syn-collisional crustal thickening and post-collisional thinning were documented in this orogen. The time scale of the collisional events could be constrained by the ages of regional amphibolite-facies metamorphic rocks and gneissic S-type granites (e.g., 460–440 Ma, Li et al., 2010). While the approximate time when the region began to shift into an extensional geological setting is still under debate (e.g., Huang and Wang, 2019; Xin et al., 2020). Some previous studies suggested the hornblende bearing I-type granites and associated mafic rocks (442–430 Ma) were produced in an extensional setting caused by lithospheric delamination (e.g., Zhong et al., 2012; Zhang et al., 2015). For instance, Zhang et al. (2015) suggest an extensional tectonic regime has developed from the beginning of the Silurian (442 Ma) with the occurrence of Guiyang I-type granites and associated Dakang mafic-felsic intrusion. Others regarded the occurrence of the A-type granites (Figures 1, 400–415 Ma) as the mark of the extensional setting (Feng et al., 2014; Li et al., 2016b; Cai et al., 2017; Xin et al., 2020). The transitional time defined by the A-type granites (ca. 415 Ma) is incompatible with the timing defined by the I-type granites and the

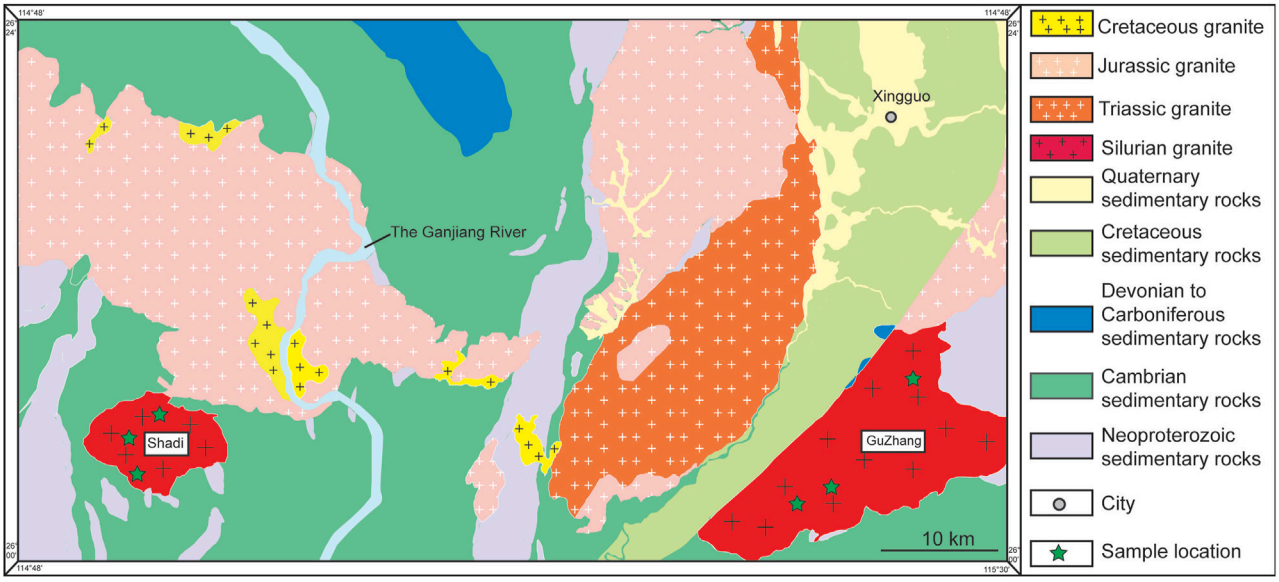

FIGURE 2
Geological map of the two A-type granitic plutons in this study. Both plutons intruded into the Neoproterozoic to Cambrian strata and have fault contact with the younger wall rocks.

contemporaneous mafic rocks (ca. 435 Ma), which require urgent constraint.

In this study, we identified two new A-type granites with ages of 430 Ma in the Nanling region. This new finding, which is in agreement with the presence of I-type granites and contemporaneous mafic-felsic complex, suggests that the Wuyi-Nanling-Yunkai orogeny had changed from compressional setting to an extensional setting at least from 430 Ma.

2 Geological background and sample introduction

The South China Block has recorded two major orogenic events before the Carboniferous era: the Neoproterozoic Jiangnan orogeny and the Early Paleozoic Wuyi-Nanling-Yunkai orogeny (Zhao et al., 2022). The Jiangnan Orogen was formed at 1.0–0.82 Ga during the assemblage of the Yangtze and Cathaysia block (Yao et al., 2019) and is characterized by the occurrence of arc-related magmatic rocks with highly depleted Nd-Hf isotopes (Li et al., 2009). However, early Paleozoic mafic rocks in the Wuyi-Nanling-Yunkai orogeny have slightly enriched to moderately depleted Nd-Hf isotopes (Xu and Xu, 2017), and were suggested to be mainly derived from a lithospheric mantle that had been metasomatized by the Neoproterozoic subducted crustal materials (e.g., Wang et al., 2013). These rare mafic rocks have a total outcrop of ca. 50 Km^2 (gabbros, with minor basalt and hornblende, Shu et al., 2020), with the ages varying from 443 to 400 Ma.

More than 200 Ordovician-Devonian granitic plutons have been found in the South China Block, with large proportions of S-, a few I- and minor A-type granites. These granitic rocks have zircon $^{238}U/^{206}Pb$ ages ranging from 464 to 381 Ma (e.g., Zhang et al., 2010; Huang et al., 2013; Cai et al., 2017) and made up the vast majority proportion of the magmatic rocks during the orogeny. The S- type granites have zircon $^{238}U/^{206}Pb$ ages from 464 to 401 Ma (e.g., Huang and Wang, 2019), and the I-type granites have zircon $^{238}U/^{206}Pb$ ages from 442 to 381 Ma (e.g., Zhao et al., 2013; Xu and Xu, 2015). Only four A-type granitic plutons have been reported, with zircon $^{238}U/^{206}Pb$ ages from 415 to 400 Ma (Feng et al., 2014; Li et al., 2016b; Cai et al., 2017; Xin et al., 2020).

The newly identified A-type granites, including two plutons named Guzhang and Shadi, are located in the middle part of the early Paleozoic Wuyi-Nanling-Yukai orogeny (Figure 2). The Guzhang granite has an outcrop of ca. 208 km^2 and Shadi granite has an outcrop of ca. 54 Km^2. The Guzhang and Shadi granitic pluton intruded into the Cambrian and Neoproterozoic basement rocks. The Cambrian rocks are mainly composed of quartz greywacke and carbonaceous slates and the Precambrian rocks are composed of tuffaceous sandstone. Hornfels is found in the granites and basement rocks contact zone.

The Guzhang pluton is mainly porphyritic biotite granite with minor two mica granite (Figures 3A–F). The phenocrysts are composed of plagioclase and K-spar, with 2–4 cm in length (Figure 3). It contains K-spar (33%–44%), plagioclase (20%–25%), quartz (20%–25%), biotite (5%–9%) and muscovite (2%–4%). The K-Spars are plate-shaped, dominated by micro-plagioclases, followed by perthites (Figure 3E). Lattice twinning and striped twinning are developed in those feldspars. Plagioclases are characterized by polysynthetic twinning (Figure 3C). The perthites and interstitial biotites indicate that crystallization occurred under anhydrous and high-temperature conditions (Philpotts, 1990). The accessory minerals are mainly zircons, apatites, Fe-Ti oxides with minor fluorite, and tourmaline. The Shadi granite is mainly composed of fine to coarse-grain biotite granite with a porphyritic texture (Figures 3G–I). The phenocrysts are composed of coarse gain (0.5–2 cm) plagioclase, K-spar and

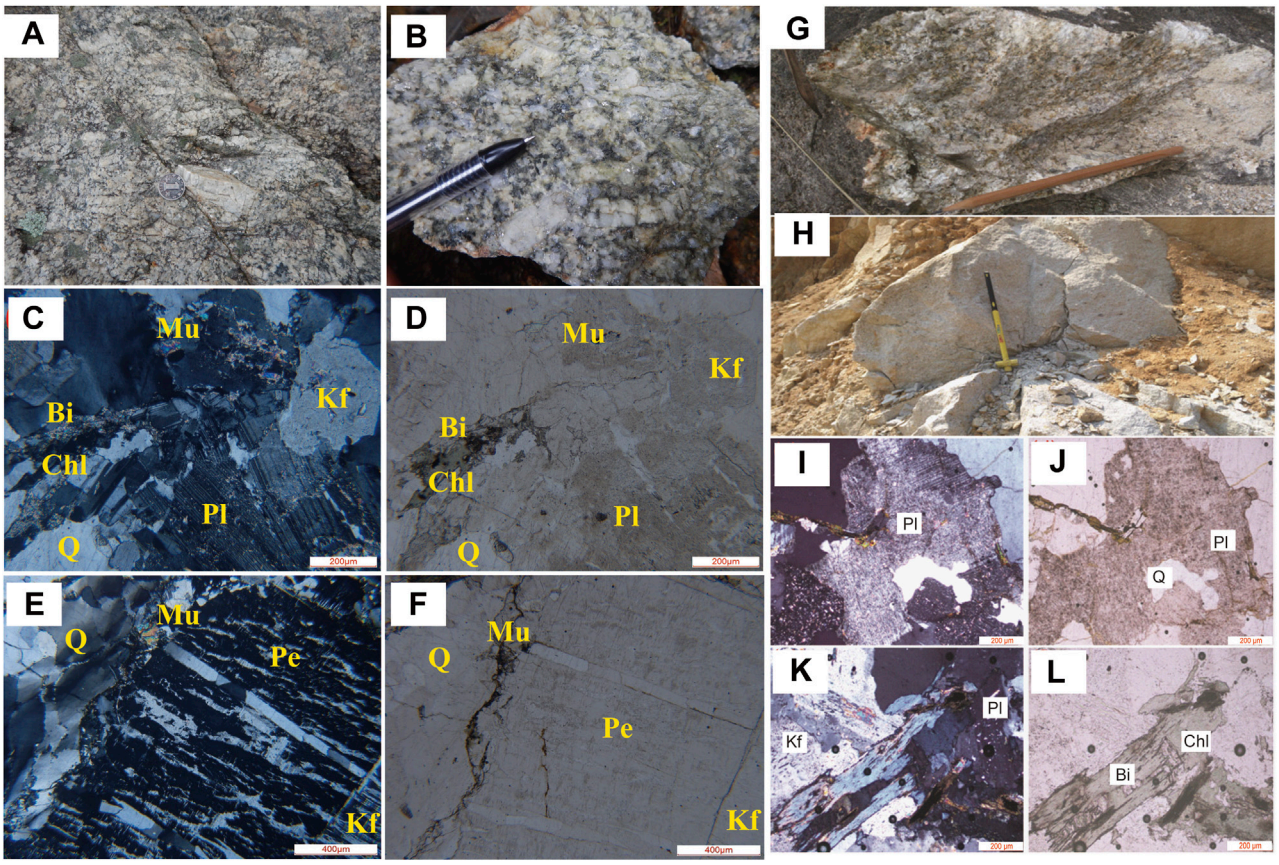

FIGURE 3
Photos from the field and thin sections for samples collected at the Guzhang **(A–F)** and Shadi granites **(G–L)**. The typical porphyritic structure can be seen in the hand specimen **(B)**. Perthites and interstitial biotites are common in both plutons. Abbreviation: Bi= Biotite; Q = Quartz; Kf = K-feldspar; Pl = Plagioclase; Mu = Muscovite; Chl= chlorite.

minor quartz with middle to fine grain (<3 mm) plagioclase (25%–31%), K-spar (25%–30%), quartz (20%–25%), biotite (6%), muscovite (2%) as matrixes. The perthites and interstitial biotites are also developed in this pluton. The accessory minerals are mainly zircons, apatites, and Fe-Ti oxides. We collected 12 samples from Guzhang and Shadi pluton for whole rock analysis and five samples for the zircon U-Pb dating and Lu-Hf isotopic analysis.

3 Analytical methods

3.1 Zircon U-Pb dating

Zircon grains were isolated using density and magnetic separation techniques. Zircons were mounted into an epoxy resin disk and polished to expose their surfaces. After photographing in both reflected and transmitted light, CL (cathode luminescence) imaging was taken by a JSM6510 SEM attached to a Gatan CL detector. Zircon U-Pb isotopic analyses were carried out on the transparent zircons without fracture or mineral inclusion using a Thermo X2 ICP-MS housed at the Testing Center of Shandong Bureau of China Metallurgical Geology Bureau, Jinan, Shandong province. The mounted zircon grains were ablated using an attached Coherent Geolas Pro 193 nm laser ablation system with a spot diameter of 30 μm. Ablation occurred in intervals of ten sample zircons, directly preceded and followed by two 91,500 standard zircons and one artificial glass 610. The analyzed results of the 91,500 fall into the ranges of the long-term test values of the Lab, with the uncertainty of 1.5% (1 RSD) for most of the $^{206}Pb/^{238}U$ measurement and are listed in Supplementary Table S1. Detailed instrument conditions and data acquisition have been described by Li et al. (2016a). The ICPMSDataCal 8.0 (Liu et al., 2010) was used to select offline raw data, integrate background and analytical signals, and time drift correct and quantitative calibrate U-Pb isotopes. The common lead correction was made following the method of Anderson (2002). The age distributions are visually compared using probability density plots (PDPs; Ludwig, 2003). Weighted average age calculation was made using Isoplot 3.23 (Ludwig, 2003).

3.2 Whole rock major and trace element geochemistry

All samples were prepared by crushing them in an agate shatter box. Major elements were analyzed using an Axios 4.0 X-ray

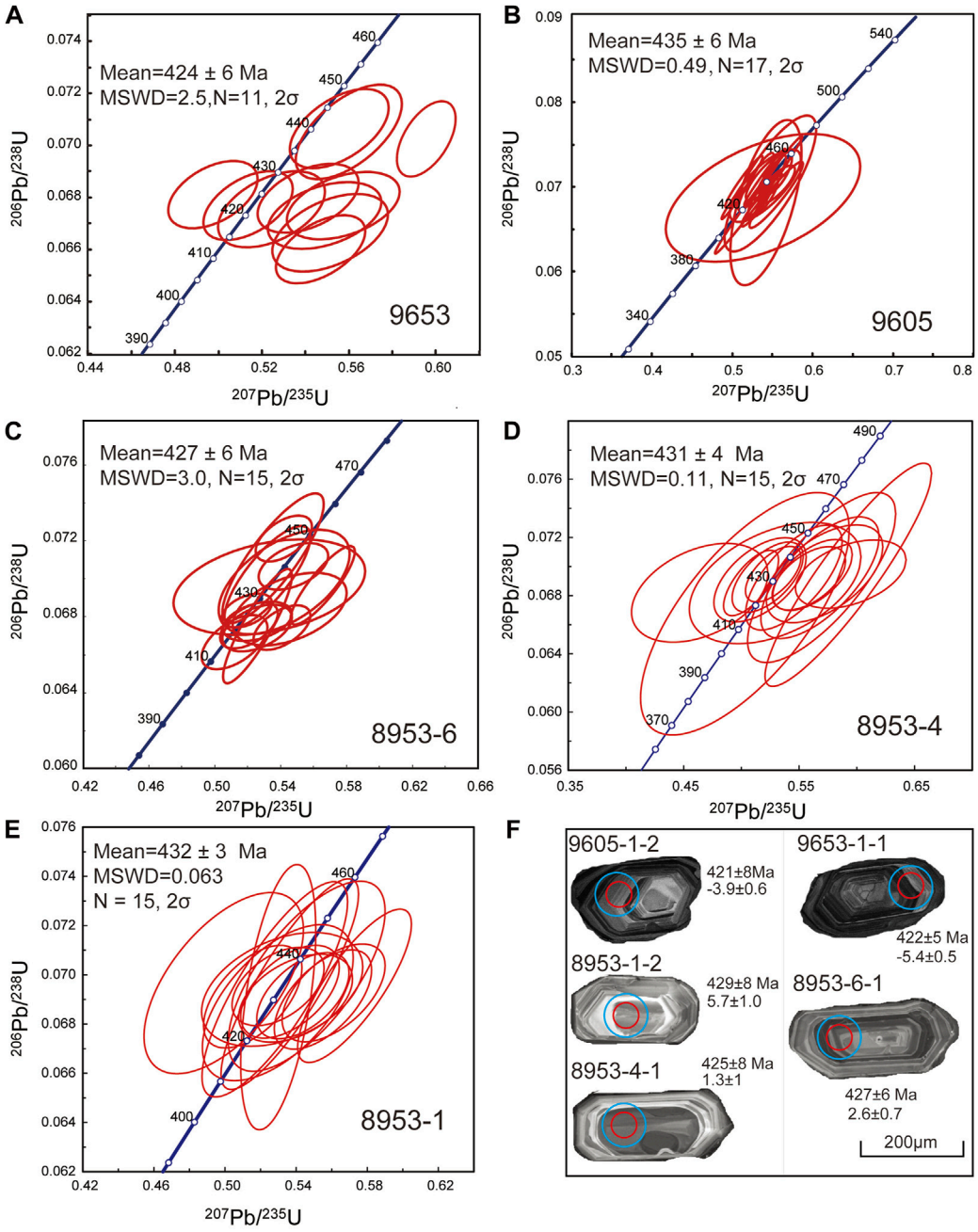

FIGURE 4
Zircon U-Pb dating Concordia diagrams **(A-E)** and representative cathode luminescence photos **(F)**. The small red circle is the zircon U-Pb analysis position and the big blue circle is the position of Lu-Hf isotope analysis.

fluorescence spectrometer (XRF) at the Testing Center of Shandong Bureau of China Metallurgical Geology Bureau, Jinan, Shandong province, following the procedures described by Franzini et al. (1972), with analytical precision better than 1%. Rare earth elements and other trace elements from the rocks were analyzed using ICP-MS (Thermo Fisher icap Q) techniques at the Testing Center of Shandong Bureau of China Metallurgical Geology Bureau, Jinan, Shandong province. The precisions for most elements are better than 5% (1SE).

3.3 Zircon Lu-Hf isotopic composition

Zircons Hf isotope analyses were carried out using a Neptune Plus MC-ICP-MS equipped with a GeoLas Pro193 nm laser at MiDeR, Nanjing University. The diameter is 44 μm with a pulse rate of 10 Hz, and beam energy of 5 J/cm^2. Only zircon grains with concordant ages and suitable sites for Hf analyses were analyzed. The zircon standard 91,500 was analyzed during the analytical session, which yielded a $^{176}Hf/^{177}Hf$ ratio of 0.282310 ± 9

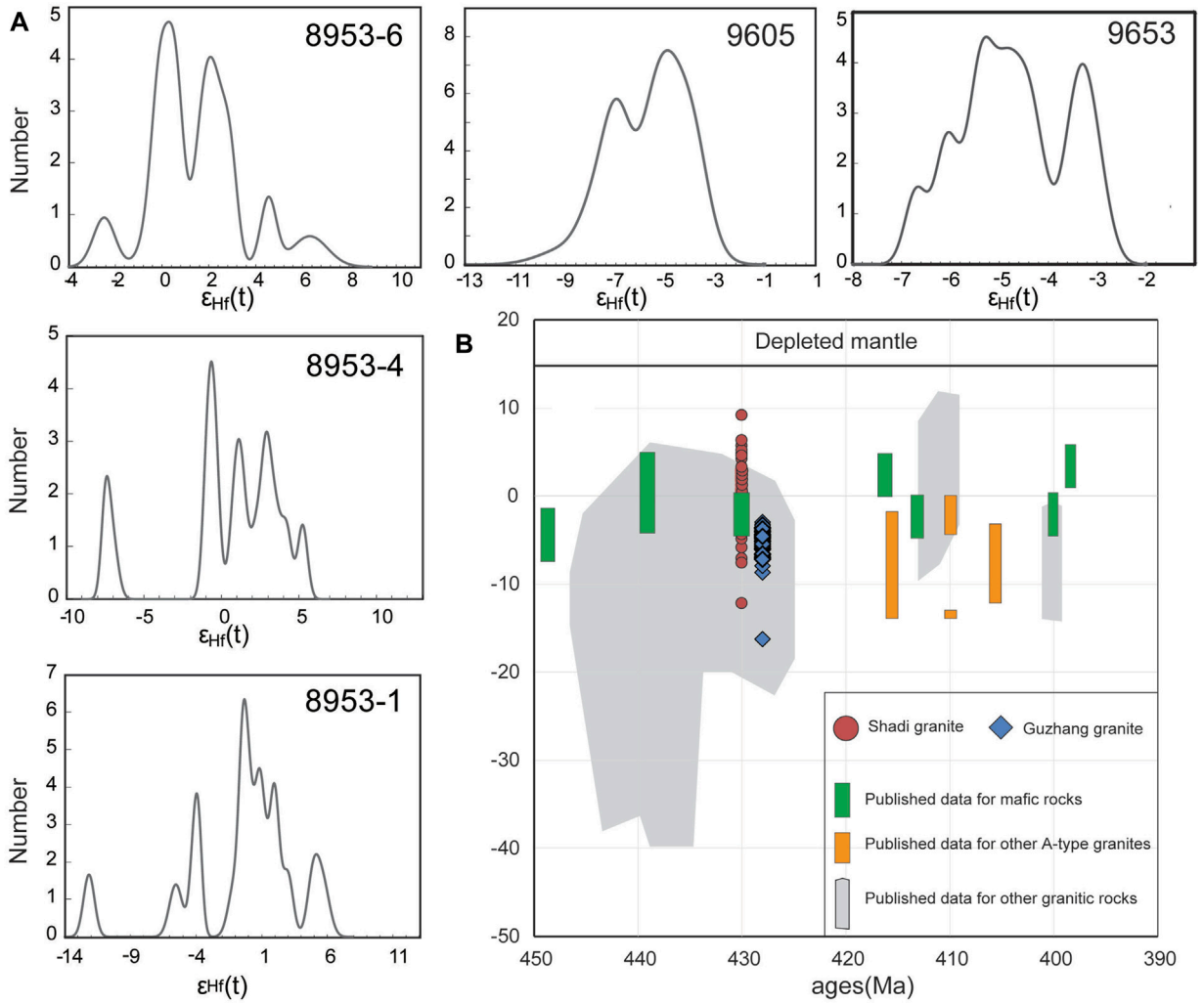

FIGURE 5
Zircon Hf isotopic composition from Guzhang and Shadi plutons. The ranges of the $\varepsilon_{Hf}(t)$ values for other granitic rocks **(B)** are from Huang and Wang et al., 2018; A-type granites are from Xin et al., 2020. Because the mafic rocks generally lack zircons, the $\varepsilon_{Hf}(t)$ values of mafic rocks are recalculated from the data source in Shu et al., 2021 by assuming the Nd-Hf isotopes are coupled (εHf=1.36*εNd+3; Vervoort et al., 1999). The Nd-Hf relationship of early Paleozoic magmatic rocks was discussed by Xia et al., 2014.

(N = 34). The calculation of εHf (t) value and T_{DM} used the following parameters: $^{\lambda}$Lu = 1.867 × 10^{-11} a^{-1} (^{176}Lu/^{177}Hf)$_{CHUR}$ = 0.0336 and (^{176}Hf/^{177}Hf)$_{CHUR}$ = 0.282785, (^{176}Lu/^{177}Hf)$_{DM}$ = 0.0384 and (^{176}Hf/^{177}Hf)$_{DM}$ = 0.28325 (Griffin et al., 2000). The average crustal ^{176}Lu/^{177}Hf value used for TDM calculations is 0.015 (Griffin et al., 2002).

4 Results

4.1 Zircon U-Pb ages and Lu-Hf isotopic composition

4.1.1 Guzhang granite

Zircons from the Guzhang pluton are euhedral, with long axis lengths from 100 to 200 μm, and aspect ratios from 1:2–1:4. These zircons have clear fine magmatic oscillation zones, which is a typical feature of zircon in the felsic rocks (Figures 4E, F e.g., Shu et al., 2011). Sixteen zircon grains were analyzed from sample 9653. Four of the results are discordant and one grain is inherited zircon. These zircons have low Th, U concentrations (<500 ppm), with Th/U ratios from 0.13 to 1.05, and are of magmatic origin (Hoskin and Schaltegger, 2003). Eleven zircon grains yield a weighted average ^{206}Pb/^{238}U ages 424 ± 6 Ma (Figure 4A, MSWD = 2.9, 2σ). The ^{206}Pb/^{238}U age of the inherited zircon is 950 ± 18 Ma. Most zircons from sample 9605 have Th/U ratios larger than 0.3, which indicates these zircons are of magmatic origin. Except for one inherited zircon have the ^{206}Pb/^{238}U ages of 654 ± 17 Ma, other zircons yield a concordant weight average ^{206}Pb/^{238}U ages of 435 ± 6 Ma (Figure 4B, n = 17, MSWD = 0.49, 2σ).

Zircon Hf isotopes from both samples of Guzhang pluton have similar values (Figure 5). The zircon $\varepsilon_{Hf}(t)$ values from sample 9605 are concentrated from −8.7 to −3.9 (n = 17), with a peak value close to −5. The T_{DM2} ages (two-stage model ages relative to the

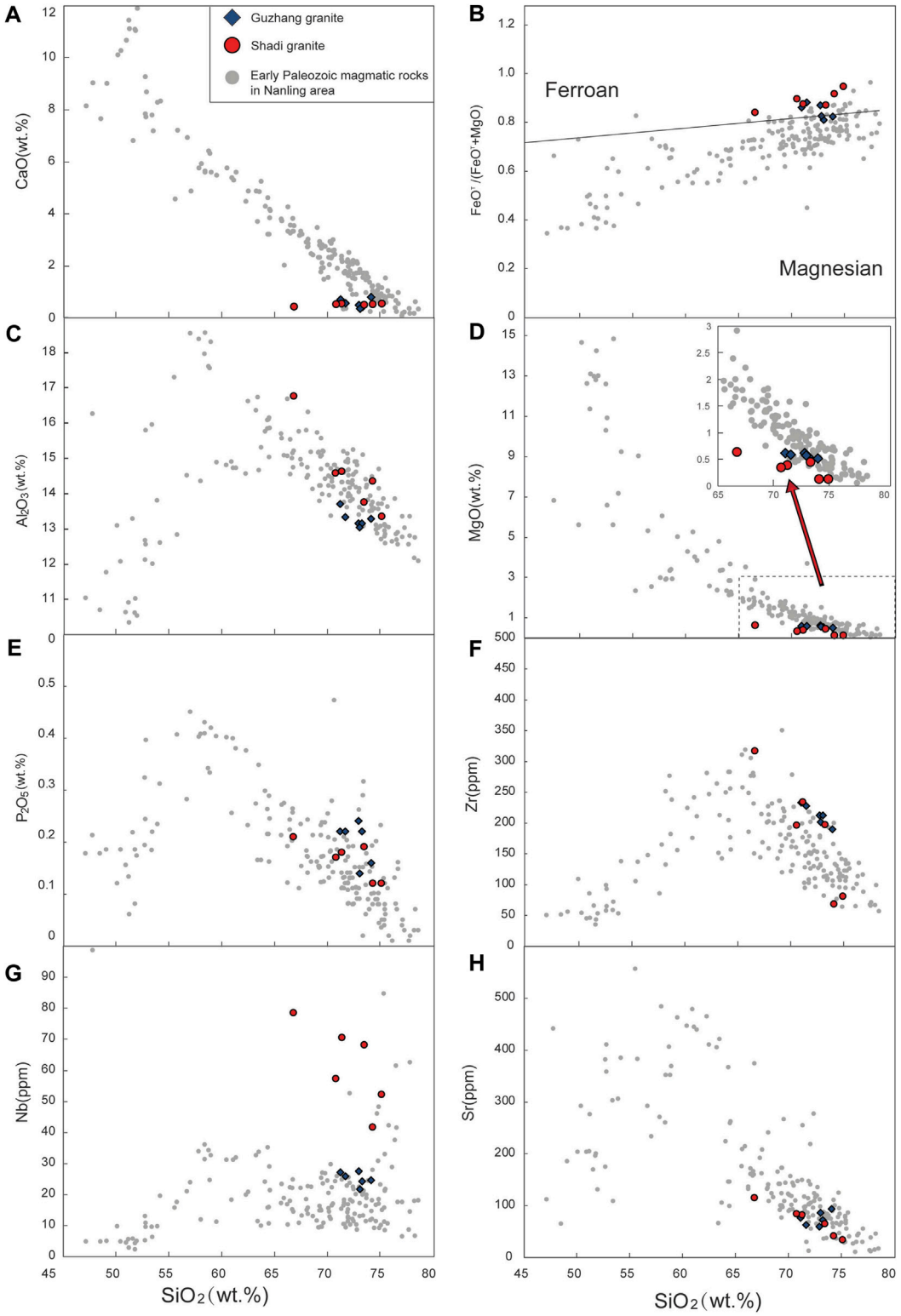

FIGURE 6
Harker diagrams for representative major **(A-E)** and trace elements **(F-H)** from the Shadi and Guzhang plutons.The coeval magmatic rock samples from the Nanling area are also plotted for comparison and the detailed data are listed in the appendix in Shu et al., 2021.

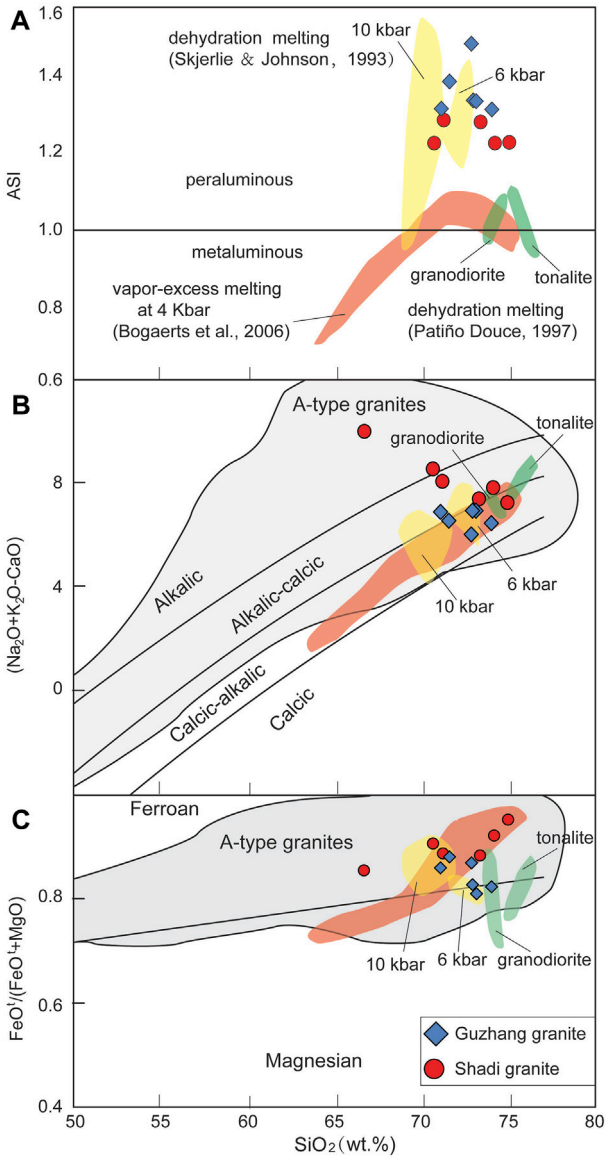

FIGURE 7
Compositional trends of melts from partial melting experiments on quartzofeldspathic rocks. **(A)** ASI [aluminium saturation index; Al/(Ca −1.67P+Na+K)] vs. SiO_2; **(B)** Na_2O+K_2O-CaO vs. SiO_2 **(C)** $(FeO^{total})/(FeO^{total}+MgO)$ vs. SiO_2. Modified from Frost and Frost, 2011. The colored area in figure b and c is the same as marked in Figure A.

depleted mantle) are from 1.63 to 1.95 Ga. The inherited zircon from 9605 has $\varepsilon_{Hf}(t = 654\ Ma)$ value of −0.2 ± 0.6. The zircon $\varepsilon_{Hf}(t)$ values from sample 9653 have more narrow ranges, varying from −6.7 to −3.0 (n = 15), with a peak value close to −4, corresponding to the T_{DM2} ages from 1.60 to 1.81 Ga. The inherited zircon from 9653 has $\varepsilon_{Hf}(t = 950\ Ma)$ value of 7.3 ± 0.5.

4.1.2 Shadi granite

Zircon samples 8953–1, 8953–4, and 8953–6 were analyzed from the Shadi pluton. The zircon grains in the Shadi granites from all samples are euhedral with clear fine magmatic oscillation zones. The grain sizes vary from 100 to 200 μm with an aspect ratio from 1:2 to 1:4. Most of the zircons have Th/U ratios from 0.2 to 0.6. which indicates they are of magmatic origin. We analyzed 16 grains with U-Pb and Lu-Hf isotopes for each sample. The concordant weighted average $^{206}Pb/^{238}U$ ages for those samples are 427 ± 6 Ma (Figure 4C, 8953–6, n = 15, MSWD = 0.3, 2σ), 431 ± 4 Ma (Figure 4D, 8953–4, n = 15, MSWD = 0.11, 2σ), and 432 ± 3 Ma (Figure 4E, 8953–1, n = 15, MSWD = 0.063, 2σ). Only one inherited zircon was found in sample 8953–6, with the $^{206}Pb/^{238}U$ ages of 960 ± 14 Ma.

Zircon Lu-Hf isotopes in the three samples have similar peak values (Figure 5). Except for one grain have $\varepsilon_{Hf}(t)$ of −12 ± 0.8, other zircons from sample 8953–1 have $\varepsilon_{Hf}(t)$ values ranging from −5.5–5.7 (n = 15), with a peak of 1, corresponding to the T_{DM2} ages of 1.03–1.75 Ga. Two zircons in 8953–4 have lower $\varepsilon_{Hf}(t)$ of −7.1 ± 0.8 and −7.5 ± 0.6, while other Zircons in 8953–4 have $\varepsilon_{Hf}(t)$ values concentrated from −0.9 to 5.2 (n = 13), with peak value close to 1, corresponding to the T_{DM2} ages of 1.06–1.45 Ga. All zircon in 8953–6 has $\varepsilon_{Hf}(t)$ values concentrated from −2.5 to 6.3 (n = 15), with a peak close to 2, corresponding to the T_{DM2} ages of 0.98–1.56 Ga. The inherited zircon from sample 8953–6 has $\varepsilon_{Hf}(t = 960\ Ma)$ values of 9.2 ± 0.6.

4.2 Major element geochemistry

The Guzhang granite is characterized by high SiO_2 (71.14–74.07 wt%), FeO^t (2.35–4.37 wt%), K_2O (3.90–4.64 wt%), Na_2O (2.67–3.02 wt%), moderate P_2O_5 (0.14–0.24 wt%), Al_2O_3 (13.04–13.71 wt%) and low CaO (0.37–0.81 wt%), MgO (0.52–0.62 wt%) contents (Supplementary Table S1, Figure 6). It shows strongly peraluminous character, with obvious high ASI values which range from 1.21 to 1.38. Samples from the Guzhang granite were plotted in the calcic-alkalic ferroan A-type field due to the high $FeO^t/(FeO^t + MgO)$ ratios (0.82–0.88) (Figure 7; Frost and Frost, 2011). The Shadi pluton has SiO_2 contents that range from 66.76 to 75.07 wt%, with lower FeO^t (1.32–3.44 wt%), CaO (0.44–0.54 wt%), moderate P_2O_5 (0.12–0.22 wt%) and higher K_2O (4.30–6.14 wt%) and Na_2O (2.92–5.02 wt%) contents. The Shadi granite has mildly high ASI values (1.12–1.22) and also belongs to the peraluminous series. It has $FeO^t/(FeO^t+MgO)$ values varying from 0.85 to 0.95, slightly higher than the Guzhang granites. Both Guzhang and Shadi plutons have obvious high $FeO^t/(FeO^t+MgO)$ values and low Cao and MgO contents compared with coeval granitic rocks in the orogeny at the same SiO_2 (Figures 6A,B,D).

4.3 Trace elements and REEs

Samples from Guzhang have higher concentrations of high-field-strength elements (HFSEs, e.g., Nb, Zr, Figures 6F,G) when compared with other coeval granites in the Nanling area (Xu and Xu, 2015). Primitive mantle normalized spider diagrams exhibit strong enrichment in Rb, Th, U, and Nd as well as clear negative anomalies in Ba, Nb, Sr, P, Eu, and Ti. The Rare earth element (REE) abundances vary from 152 to 212 ppm with light REE enrichment, significant negative Eu anomalies, and flat-sloping heavy REE patterns (Figures 8A, B). Samples from the Shadi have similar trace element features with the Guzhang granite, which are featured by the enrichment of HFSEs and depletion of

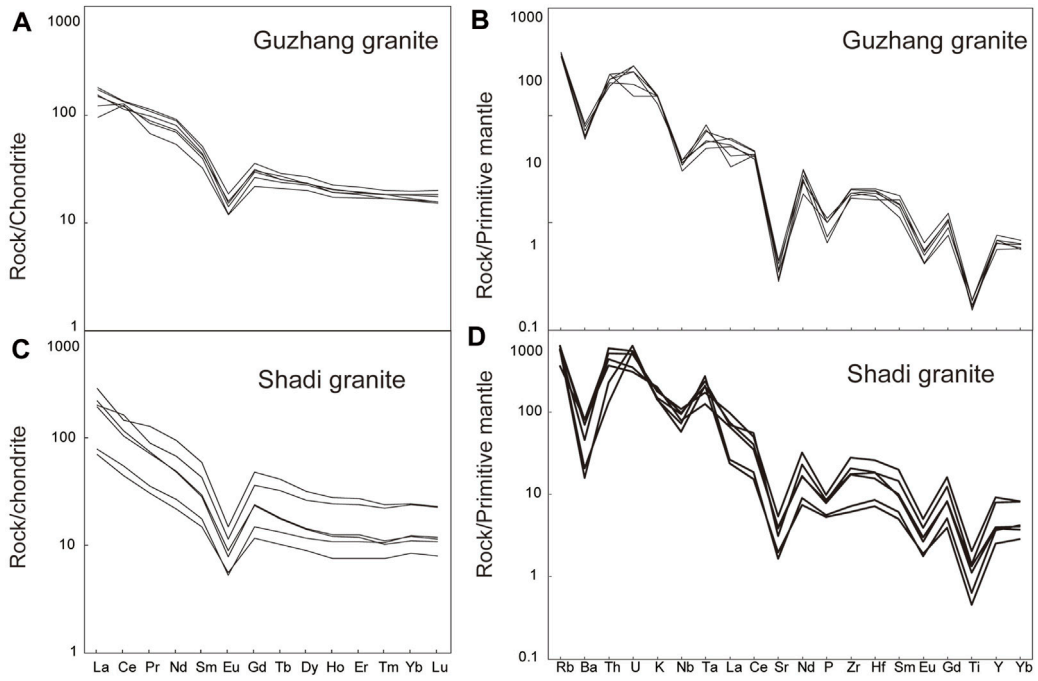

FIGURE 8
C1-Chondrite normalized REE patterns **(A–C)** and primitive mantle normalized alteration resistant trace element pattern **(B–D)** for the samples from the Guzhang and Shadi plutons. Chondrite and primitive mantle compositions are from Sun and McDonough (1989).

Ba, Nb, Sr, Eu, and Ti. The total REEs of Shadi granites have larger variations than that of Guzhang granites, from 67 to 254 ppm. It also shows strong negative Eu abnormally on the chondrite normalized REEs patterns (Figures 8C, D). The heavy depletion of Eu, Ba, and Sr in both plutons indicates that the feldspars played a significant role during the magma generation, either as residuals in the source or as fractionated minerals.

5 Discussions

5.1 Genesis type

The majority of granites can commonly be classified as I-, S-, or A-types based on mineral combinations and geochemical characteristics (Bonin, 2007). Chappell and white (1974) divided the granites in the Lachlan fold belt into I- and S-type. The I-type granites are characteristic of low SiO_2 contents, ASI values (normally <1.1), depleted isotopes (e.g., Sr, Nd, Hf), and the appearance of hornblendes, derived from mainly meta-igneous rock sources. The S-type granites are featured by high ASI values (normally >1.1), enriched isotopes with the appearance of garnet and/or cordierite, and are suggested to be mainly derived from meta-sedimentary rocks. It is worth noting that the mineralogical and geochemical characteristics mentioned above are not solid standards for the classification of granite types. For example, aluminum-rich minerals such as primary garnet can also be found in weak peraluminous and even meta-aluminous granites (Chappell, 1999). The geochemical characteristics of A-type granites differ from those of I- and S-type granites (e.g., high contents of HFSEs and Ga/Al ratios), and the geochemical parameters used to define A-type granite are unambiguous. (Loiselle and wones, 1979; Eby, 1990; Creaser et al., 1991; Bonin, 2007).

Even the high ASI values and the existence of biotite and minor muscovite are similar to the future of some typical S-type granites (Bonin, 2007), the high formation temperatures, $FeO^{tot}/(FeO^{tot}+MgO)$ ratios, and limited inherited zircons (3 inherited zircons of 76 grains) and other features that will be discussed next preclude the S-type origin. The most noticeable characteristics of Guzhang and Shadi plutons are as follows: 1) high $FeO^{tot}/(FeO^{tot}+MgO)$ ratios and ASI values (Figures 6, 7); 2) low contents of Al_2O_3, CaO, MgO (Figure 6); 3) mildly negative to positive Zircon Hf isotopic composition (Figure 5B); 4) high HFSEs concentrations and Ga/Al ratios; 5) the occurrences of interstitial biotites and perthitic microcline; 6) lack of inherited zircons. The $FeO^{t}/(FeO^{t}+MgO)$ ratios of samples from both plutons are plotted in the ferroan A-type granites field (Figure 7C, defined by 175 A-type granites worldwide; Frost et al., 2001) and are distinguishable compared with the magmatic rocks that formed during 460–400 Ma in Nanling area (Figure 6B). Most of the samples were plotted near or in the field of A-type granites on different chemical diagrams because of the high HFSEs concentrations and 10,000*Ga/Al ratios (Figure 9).

Besides the distinct A-type granite geochemical features, these two plutons also have high Zr saturation temperatures. The Guzhang granite has whole rock Zr saturation temperatures from 820°C to 840°C (Supplementary Table S1, M[(Na + K + 2*Ca)/(Al*Si)]=1.1–1.2; Watson and Harrison, 2005) and four of six samples from the Shadi granite (M=1.2–1.4) have temperatures from 813°C to 845°C (Figure 10A). The other two low-

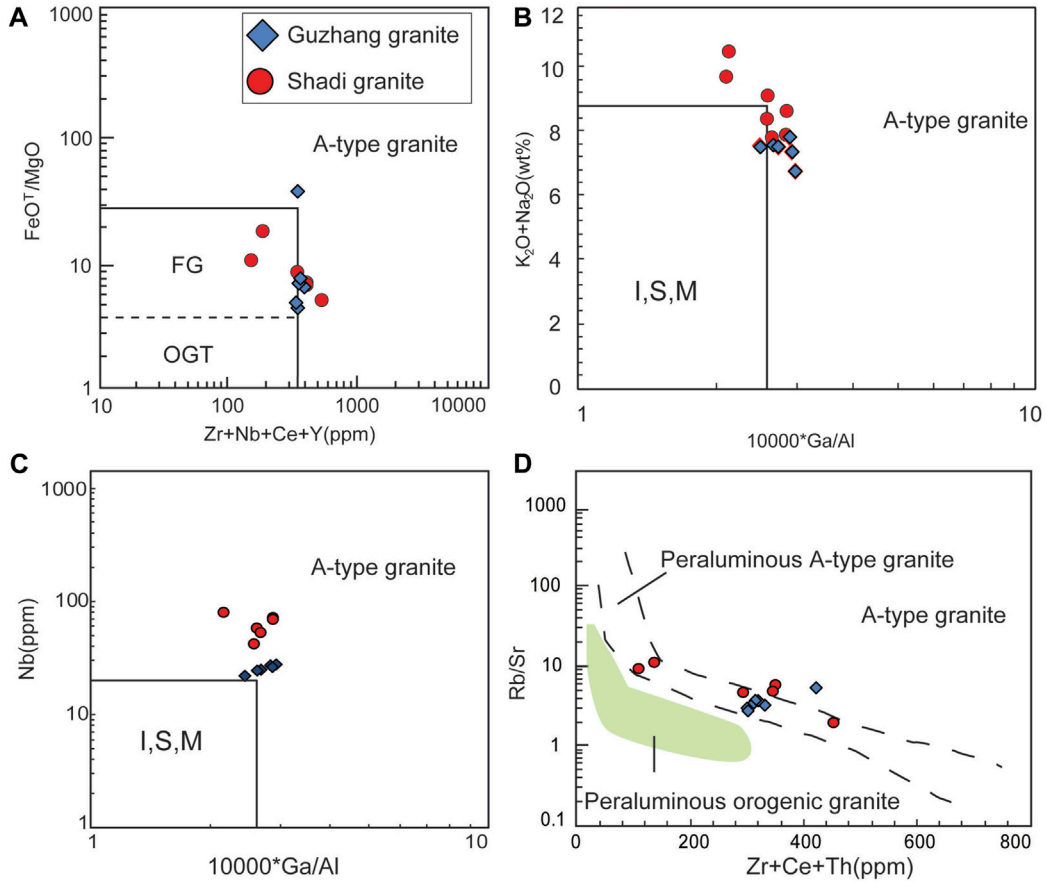

FIGURE 9
Chemical classification diagrams for granites: **(A)** (FeO^T/MgO) vs. (Zr + Nb+ Ce + Y); **(B)** (K_2O+ Na_2O) vs 10,000 Ga/Al; **(C)** Nb vs. (Zr + Nb + Ce + Y); **(D)** Rh/Sr vs. (Zr + Ce + Th) (Whalen et al., 1987 and Cámera et al., 2017). FG: Fractionated granites; OGT: unfractionated M-, I- and, S-type granites.

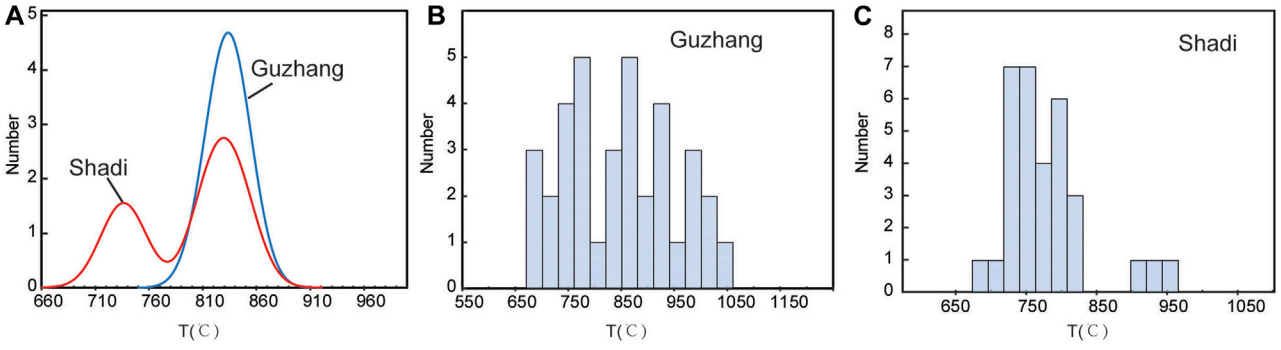

FIGURE 10
Calculated temperatures for samples and zircons from the Guzhang and Shadi plutons. Figure **(A)** is the Zr saturation temperature calculated from whole rock geochemistry. Figure **(B, C)** are the temperatures calculated from the Ti concentrations in zircons.

temperature samples (ca. 750°C) from the Shadi pluton have the highest SiO_2 and lowest Zr (68 and 80 ppm) and Ti contents, which may cause by fractional crystallization. The zircon Ti thermometry is also used to calculate the zircon crystallization temperature. A new correction of Ti in zircon temperature calculation was made by Schiller and Finger (2019), and they suggest the zircon temperatures in most A-type granites were underestimated. The zircons from Guzhang and Shadi granite have saturation temperatures from 700°C to 1000°C and 700°C–950°C, respectively (Figure 10B). Combined with the occurrences of interstitial biotites and

perthitic microcline, it may be concluded that both plutons evolved under anhydrous conditions at high temperatures. All of the aforementioned characteristics suggest that these two granitic plutons are ferroan A-type.

5.2 Origin of the two peraluminous A-type granites

There is no consensus on the origin of the A-type granites, especially on the source (Bonin, 2007). Even Frost and Frost (2011) suggested using the term "Ferroan granites" instead of "A-type granites" for some reason, the term "A-type granite" is still more popular than the "Ferron granites" nowadays. The main petrogenetic models for the A-type granite include 1) Partial melting of lower crust rocks that had been granulitized during an earlier thermal event (Collins et al., 1982; Feng et al., 2014); 2) Direct differentiation from the mantle-derived basaltic magma (Frost and Frost, 2011; Girei et al., 2019; Jiang et al., 2022); 3) Partial melting of the quartzofeldspathic rocks (Patiño Douce, 1997; Bogaerts et al., 2006; Kong et al., 2018; Li et al., 2018a; Li et al., 2018b; Li et al., 2018c); 4) Magma mixing from anatectic granitic and mantle-derive mafic magmas (Dahlquist et al., 2010; Cámera et al., 2017).

The granulite model with pre-extraction of I-type granitic melt was argued by some scholars for such melts would have low Fe/Mg and $(Na_2O+K_2O)/Al_2O_3$ ratios that differ from typical A-type granites (e.g., Creaser et al., 1991; Frost and Frost, 2011; Jiang et al., 2022). However, some studies suggested that the early Paleozoic A-type granites in the Wuyi-Nanling-Yunkai orogen were derived from mainly granulitic rock sources, such as granulitic meta-igneous rocks (Cai et al., 2017), granulitic meta-sedimentary rocks (Feng et al., 2014) or granulite that had extracted S-type granitic magma (Xin et al., 2020). The main reason is due to the low water affinity of the granulite which seems as a suitable source for the anhydrous A-type magmas. We are not intended to connect the Guzhang and Shadi plutons with the granulite source, since it is not a necessary factor to generate the A-type granites (Creaser et al., 1991; Skjerlie and Johnston, 1993).

The Guzhang granite has negative zircon $\varepsilon_{Hf}(t)$ values (−8.7—−3.0) that are unlikely derived from a coeval mantle-derived mafic magma (Figure 5B). The Shadi granite has higher $\varepsilon_{Hf}(t)$ values that overlap with the ranges of coeval mafic rocks, which can be derived from the differentiation of the basaltic rocks isotopically (Figure 5B). However, A-type granites that derived from differentiation of the basaltic magma are generally metaluminous and commonly found in association with mafic intrusions (Mccurry et al., 2008). Both Guzhang and Shadi plutons are peraluminous and not found to be associated with mafic intrusion or mafic enclaves. Thus, they are not likely derived from the direct fractionation of mafic magmas. Besides, zircon $\varepsilon_{Hf}(t)$ values from both plutons have large ranges, up to 10 ε units. The large ranges in zircon $\varepsilon_{Hf}(t)$ are either caused by magma mixing (Griffin et al., 2002) or by disequilibrium melting during the crustal anataxis (Tong et al., 2021). The magma mixing model is not favored here because mafic magmas mostly have low ASI values (<0.8) and the magma produced by pure mixing can hardly achieve the strong peraluminous affinity of our samples, while source mixing is more plausible.

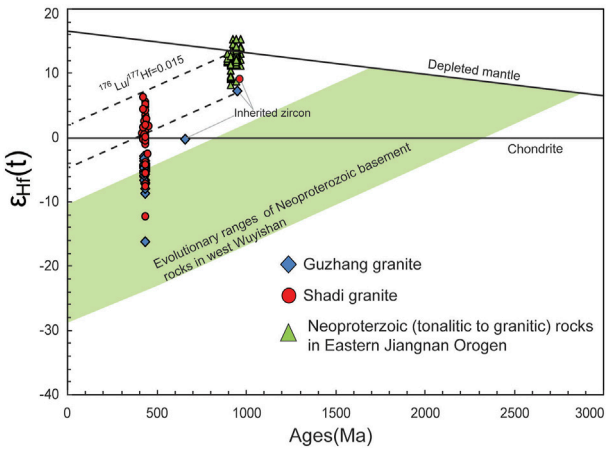

FIGURE 11
$\varepsilon_{Hf}(t)$ vs ages (Ma) diagrams. The Neoproterozoic data is from Li et al., 2009; Chen et al., 2009. The ranges of Neoproterozoic basement rocks in the west Wuyishan area are from Xin et al. (2020). Both plutons are not likely derived from the old basement rocks for the higher $\varepsilon_{Hf}(t)$ values. The Shadi granites can be mainly derived from a source similar to the Neoproterozoic juvenile tonalitic rocks in the eastern Jiangnan Orogen while the Guzhang granites have a mixed source with more old crustal materials.

Partial melting of mainly quartzofeldspathic rocks during crustal anataxis is a possible way to generate the A-type granites (Frost and frost, 2011). For instance, dehydration melting of F-rich tonalitic gneiss at mid-crustal pressures can generate strong peraluminous A-type granites (Figure 7; Skjerlie and Johnston, 1993). The Guzhang granite has mildly negative $\varepsilon_{Hf}(t)$ values (−8.7—−3.0), which are higher than most coeval granitic plutons, especially the typical S-type granites ($\varepsilon_{Hf}(t)$ = −34.2—−0.2; n=963, median = −8.4; Xin et al., 2020) and also the Neoproterozoic basement rocks in the west Wuyishan area. (Figure 11). Thus, it is unlikely derived from a source that is dominated by old metasedimentary rock. Zircon from the Shadi pluton has positive $\varepsilon_{Hf}(t)$ values up to +6.3, indicating that it originated from the partial melting of more immature source rocks rather than sedimentary source rocks.

The Neoproterozoic juvenile rocks in the Jiangnan Orogen, like the tonalitic to rhyolitic magmatic rocks from Shuangxiwu and Pingshui area, seem a good candidate as the source of these A-type granites (Chen et al., 2009; Li et al., 2009). Neoproterozoic inherited zircons with depleted Hf isotopic characteristics were found in the Shadi (ε_{Hf} (t=960 Ma) = 9.2 ± 0.6) and the Guzhang pluton (ε_{Hf} (t=950 Ma) = 7.3 ± 0.5), both of which occur within the ranges of zircons from the tonalitic rocks at the eastern Jiangnan Orogen (Figure 11; Li et al., 2009). Besides, the Beiwu volcanic rocks with tonalitic composition (See Supplementary Table S2 in Li et al., 2009) have major elements similar to the starting materials used in the dehydration melting experiment in Skjerlie and Johnston, 1993. Thus, the dehydration melting of source rocks that are similar to the juvenile tonalitic rocks from the east Jiangnan Orogen can generate peraluminous Shadi A-type granite, geochemically and isotopically. Therefore, we suggest these two peraluminous granitic plutons were most likely formed by the dehydration melting of Neoproterozoic

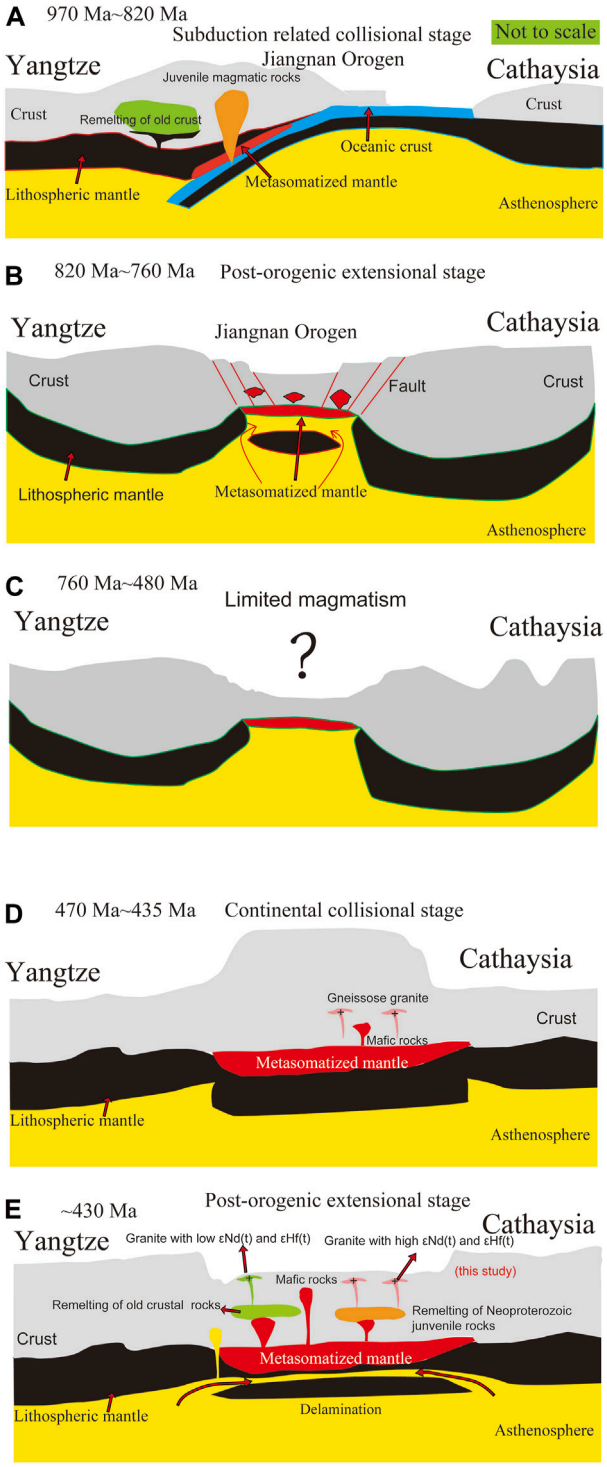

FIGURE 12
The schematic cartoons showing the tectonic evolution of SCB and the generation of the A-type granites in this study. The amalgamation of the Yangtze and the Cathaysia Block in Neoproterozoic time generated intermediate to felsic magmatic rocks with depleted Nd-Hf isotopic features **(A)**. This amalgamation was followed by a post-orogenic extension which is recorded by A-type granites and other rift-related mafic rocks **(B)**, Yao et al., 2019). However, after 760 Ma, the magmatism in SCB was limited **(C)**. Some magmatic rocks and metamorphic rocks were identified in SCB with the ages from 470 to 445 Ma and regarded as products of the continental collisional stage **(D)**. Large volumes of magmatic rocks were formed at the extensional stage (430–400 Ma) after the delamination of the thickened crust and upper lithospheric mantle **(E)**.b

juvenile tonalitic rocks with minor metasedimentary rocks at medium crust pressure, with the source of Guzhang granite containing more old metasedimentary rocks (Figure 12).

5.3 Tectonic implication

The orogeny of this early Paleozoic belt was first recognized by the mass distributions of the regional metamorphic rocks (greenschist, amphiboles, and minor granulites, Figure 1). Systematic geochronology studies of those metamorphic rocks were formed at 460–436 Ma (Yu et al., 2005; Yu et al., 2014; Li et al., 2010; Tong et al., 2021). The occurrence of high-pressure metamorphic rocks revealed crustal thickening events in the belt (Li et al., 2010; Yu et al., 2014; Tong et al., 2021). The crustal thickening events were mainly suggested to be triggered by continental collision (Charvet et al., 2010; Li et al., 2010; Yao et al., 2012; Wang et al., 2013; Shu et al., 2014; Kong et al., 2021; Zhao et al., 2022). The youngest metamorphic zircon U-Pb ages from the Yiyang granulite are at ca. 435 Ma (Yu et al., 2014) and this age may mark the end of the collision event since no metamorphic rocks with younger ages have been reported. However, the accurate transformational age of this belt from compression to extension is still debated.

A-type granites had long been recognized as derived at extensional settings (e.g., Collins et al., 1982; Forst and Forst, 2011). In collisional orogens, syn-collisional crustal thickening has been followed by delamination of substantial amounts of mantle lithosphere at the post-collisional stage (Davies and von Blanckenburg, 1995). The post-collisional extension provides a suitable environment for hot mafic magma upwelling and also the heat for melting the source rocks of A-type granites (Jiang et al., 2022). Thus, the formation ages of A-type granites are often suggested to be the time that the region changes into a strongly extensional geological background. A-type granites in SCB have previously been dated between 415 and 400 Ma, hence it was hypothesized that the Wuyi-Nanling-Yunkai orogeny transitioned from syn-orogenic crustal thickening to a post-orogenic thinning at 415 Ma. (e.g., Xin et al., 2020).

However, most studies considered the hornblende bearing I-type granites (e.g., Guiyang granite formed at 442 Ma, Zhang et al., 2015) and coeval mafic rocks (e.g., Chayuanshan high Mg basalts formed at 435 Ma, Yao et al., 2012) were produced in an extensional setting that caused by lithospheric delamination. Huang and Wang (2019) also suggested that the occurrence of massive high-K calc-alkaline I-type granites in the Xuefengshan area can exemplify the transitional period from compression to extension, with the ages of ca. 430 Ma. Besides, the gneissic S-type granites in the belt mainly have a peak age of 440 Ma, and massive S-type granites have a peak age of 430 Ma. Those massive S-type granites were also suggested to be derived during the orogenic collapse stage (Feng et al. (2014). The ages of Shadi and Guzhang A-type granites in this study are consistent with the conclusion from the S-, I- type granites and the coeval mafic rocks. Thus, we suggest that the setting of Wuyi-Nanling-Yunkai orogen had changed from compression to extensional at least at ca. 430 Ma, which is 15 Ma earlier than the previous conclusion from A-type granites.

6 Conclusion

1) We identified two new peraluminous granites in the Wuyi-Nanling-Yunkai orogen, South China. These two plutons have high $FeO^t/(FeO^t + MgO)$, Ga/Al ratios, and HFSEs concentrations with low CaO and MgO contents as well as high formation temperature, and are fitted with the affinities of A-type granites.
2) LA-ICP-MS zircon U-Pb dating results indicate the Shadi granite and the Guzhang granite were formed at 430 ± 5 Ma. Both granites can be formed by partial melting of mainly Neoproterozoic juvenile meta-tonalitic rocks at medium crust pressure while the source of Guzhang granite contains more old crustal materials. The Neoproterozoic juvenile tonalitic rocks in Jiangnan Orogen might be a significant source for the A-type granites.
3) This new finding suggests the geological setting of the Nanling area in the Wuyi-Nanling-Yunkai orogeny changed from collision to post-collisional extension no later than 430 Ma.

Data Availability Statement

The original contributions presented in the study are included in the article/Supplementary Material, further inquiries can be directed to the corresponding author.

Author contributions

X-JS, writing-original draft preparation, WJ sampling, experiment, data calculation. DW, supervision, review. CC and HW, discussion, editing, language.

Funding

This work was supported by financial support from the National Natural Science Foundation of China (41802063).

Acknowledgments

We thank Dehong Du and Jiangwei Zhang for the Discussions.

Conflict of interest

The authors declare that the research was conducted in the absence of any commercial or financial relationships that could be construed as a potential conflict of interest.

Publisher's note

Supplementary material

The Supplementary Material for this article can be found online at: https://www.frontiersin.org/articles/10.3389/feart.2023.1137157/full#supplementary-material

References

Anderson, T. (2002). Correction of common lead in U–Pb analyses that do not report 204Pb. *Chem. Geol.* 192, 59–79. doi:10.1016/S0009-2541(02)00195-X

Bogaerts, M., Scaillet, B., and VanderAuwera, J. (2006). Phase equilibria of the Lyngdal granodiorite (Norway): Implications for the origin of metaluminous ferroan granitoids. *J. Pet.* 47, 2405–2431. doi:10.1093/petrology/egl049

Bonin, B. (2007). A-type granites and related rocks; evolution of a concept, problems and prospects. *Lithos* 97, 1–29. doi:10.1016/j.lithos.2006.12.007

Cai, D. W., Tang, Y., Zhang, H., Lv, Z. H., and Liu, Y. L. (2017). Petrogenesis and tectonic setting of the devonian xiqin A-type granite in the northeastern cathaysia block, SE China. *J. Asian Earth Sci.* 141, 43–58. doi:10.1016/j.jseaes.2016.05.015

Cámera, M. M. M., Dahlquist, J. A., Basei, M. A., Galindo, C., Neto, M. D. C. C., and Facetti, N. (2017). F-rich strongly peraluminous A-type magmatism in the pre-Andean foreland Sierras Pampeanas, Argentina: Geochemical, geochronological, isotopic constraints and petrogenesis. *Lithos* 277, 210–227. doi:10.1016/j.lithos.2016.10.035

Chappell, B. W. (1999). Aluminium saturation in I-and S-type granites and the characterization of fractionated haplogranites. *Lithos* 46 (3), 535–551. doi:10.1016/s0024-4937(98)00086-3

Chappell, B. W., and White, A. J. R. (1974). Two contrasting granite types. *Pac. Geol.* 8, 173–174.

Charvet, J., Shu, L. S., Faure, M., Choulet, F., Wang, B., Lu, H. F., et al. (2010). Structural development of the lower paleozoic belt of SouthSouth China: Genesis of an intracontinental orogen. *J. Asian Earth Sci.* 39 (4), 309–330. doi:10.1016/j.jseaes.2010.03.006

Chen, Z. H., Xing, G. F., Guo, K. Y., Dong, Y. G., Chen, R., Zeng, Y., et al. (2009). Petrogenesis of the Pingshui keratophyre from Zhejiang: Zircon U–Pb age and Hf isotope constraints. *Chin. Sci. Bull.* 54, 610–617. doi:10.1007/s11434-009-0081-y

Collins, W. J., Beams, S. D., White, A. J. R., and Chappell, B. W. (1982). Nature and origin of A-type granites with particular reference to southeastern Australia. *Contrib. Mineral. Pet.* 80, 189–200. doi:10.1007/bf00374895

Creaser, R. A., Price, R. C., and Wormald, R. J. (1991). A-Type granites revisited: Assessment of a residual-source model. *Geology* 19, 163–166. doi:10.1130/0091-7613(1991)019<0163:atgrao>2.3.co;2

Dahlquist, J. A., Alasino, P. H., Eby, G. N., Galindo, C., and Casquet, C. (2010). Fault controlled carboniferous A-type magmatism in the proto-andean foreland (sierras pampeanas, Argentina): Geochemical constraints and petrogenesis. *Lithos* 115, 65–81. doi:10.1016/j.lithos.2009.11.006

Davies, J. H., and von Blanckenburg, F. (1995). Slab breakoff: A model of lithosphere detachment and its test in the magmatism and deformation of collisional orogens. *Earth Planet. Sci. Lett.* 129, 85–102. doi:10.1016/0012-821x(94)00237-s

Eby, G. N. (1990). The A-type granitoids: A review of their occurrence and chemical characteristics and speculations on their petrogenesis. *Lithos* 26, 115–134. doi:10.1016/0024-4937(90)90043-z

Feng, S. J., Zhao, K. D., Ling, H. F., Chen, P. R., Chen, W. F., Sun, T., et al. (2014). Geochronology, elemental and Nd-Hf isotopic geochemistry of Devonian A-type granites in central Jiangxi, South China: Constraints on petrogenesis and post-collisional extension of the Wuyi–Yunkai orogeny. *Lithos* 206–207, 1–18. doi:10.1016/j.lithos.2014.07.007

Franzini, M., Leoni, L., and Saitta, M. (1972). A simple method to evaluate the matrix effects in X-ray fluorescence analysis. *X-Ray Spectrom.* 1 (4), 151–154. doi:10.1002/xrs.1300010406

Frost, B. R., Arculus, R. J., Barnes, C. G., Collins, W. J., Ellis, D. J., and Frost, C. D. (2001). A geochemical classification for granitic rocks. *J. Pet.* 42, 2033–2048. doi:10.1093/petrology/42.11.2033

Frost, C. D., and Frost, B. R. (2011). On ferroan (A-type) granitoids: Their compositional variability and modes of origin. *J. Pet.* 52 (1), 39–53. doi:10.1093/petrology/egq070

Girei, M. B., Li, H., Algeo, T. J., Bonin, B., Ogunleye, P. O., Bute, S. I., et al. (2019). Petrogenesis of A-type granites associated with Sn–Nb–Zn mineralization in Ririwai complex, north-Central Nigeria: Constraints from whole-rock Sm–Nd and zircon Lu–Hf isotope systematics. *Lithos* 341, 49–70. doi:10.1016/j.lithos.2019.05.003

Griffin, W. L., Pearson, N. J., Belousova, E. A., Jackson, S. E., van Achterbergh, E., O'Reilly, S. Y., et al. (2000). The Hf isotope composition of cratonic mantle: LAM-MC-ICPMS analysis of zircon megacrysts in kimberlites. *Geochim. Cosmochim. Acta* 64 (1), 133–147. doi:10.1016/S0016-7037(99)00343–9

Griffin, W. L., Wang, X., Jackson, S. E., Pearson, N. J., O'Reilly, S. Y., Xu, X. S., et al. (2002). Zircon chemistry and magma mixing, SE China: *In-situ* analysis of Hf isotopes, tonglu and pingtan igneous complexes. *Lithos* 61, 237–269. doi:10.1016/S0024-4937(02)00082-8

Hoskin, P. W., and Schaltegger, U. (2003). The composition of zircon and igneous and metamorphic petrogenesis. *Rev. Mineral. Geochem.* 53 (1), 27–62. doi:10.2113/0530027

Huang, D. L., and Wang, X. L. (2019). Reviews of geochronology, geochemistry, and geodynamic processes of Ordovician-Devonian granitic rocks in southeast China. *J. Asian Earth Sci.* 184, 104001. doi:10.1016/j.jseaes.2019.104001

Huang, X. L., Yu, Y., Li, J., Tong, L. X., and Chen, L. L. (2013). Geochronology and petrogenesis of the early paleozoic I-type granite in the taishan area, South China: Middle-lower crustal melting during orogenic collapse. *Lithos* 177, 268–284. doi:10.1016/j.lithos.2013.07.002

Jiang, Y. H., Liu, Y. C., Han, B. N., Qing, L., and Du, F. G. (2022). Contrasting origins of A-type granites in the late triassic-early jurassic pitou complex, southern jiangxi province: Implications for mesozoic tectonic evolution in SouthSouth China. *Lithos* 426, 106794. doi:10.1016/j.lithos.2022.106794

Kong, H., Li, H., Wu, Q. H., Xi, X. S., Dick, J. M., and Gabo-Ratio, J. A. S. (2018). Co-development of Jurassic I-type and A-type granites in southern Hunan, South China: Dual control by plate subduction and intraplate mantle upwelling. *Chem. Erde – Geochem.* 78, 500–520. doi:10.1016/j.chemer.2018.08.002

Kong, H., Wu, J. H., Li, H., Chen, S. F., Liu, B., and Wang, G. (2021). Early paleozoic tectonic evolution of the SouthSouth China block: Constraints from geochemistry and geochronology of granitoids in hunan province. *Lithos* 380-381, 105891–106381. doi:10.1016/j.lithos.2020.105891

Li, F. C., Hou, M. L., Luan, R. J., Lin, P. J., Li, Z. S., Zhao, L., et al. (2016a). Optimization of analytical conditions for LA-ICP-MS and its application to zircon U–Pb dating. *Rocks Min. Anal.* 35, 17–23. doi:10.15898/j.cnki.11-2131/td.2016.01.004

Li, H., Liu, Y. H., Li, Z., Zhou, S. F., Li, X., and Wei, J. Z. (2016b). Geochemical characteristics and geological significance of granite geochronology in dayao mountain [in Chinese with English abstract]: Guangxi. *J. Guilin Uni. Tech.* 39 (1), 29–37. doi:10.3969/j.issn1674-3504.2016.01.005

Li, H., Myint, A. Z., Yonezu, K., Watanabe, K., Algeo, T. J., and Wu, J. H. (2018a). Geochemistry and U–Pb geochronology of the Wagone and Hermyingyi A-type granites, southern Myanmar: Implications for tectonic setting, magma evolution and Sn–W mineralization. *Ore Geol. Rev.* 95, 575–592. doi:10.1016/j.oregeorev.2018.03.015

Li, H., Palinkaš, L. A., Watanabe, K., and Xi, X. S. (2018b). Petrogenesis of Jurassic A-type granites associated with Cu–Mo and W–Sn deposits in the central Nanling region, South China: Relation to mantle upwelling and intra-continental extension. *Ore Geol. Rev.* 92, 449–462. doi:10.1016/j.oregeorev.2017.11.029

Li, H., Wu, J. H., Evans, N. J., Jiang, W. C., and Zhou, Z. K. (2018c). Zircon geochronology and geochemistry of the Xianghualing A-type granitic rocks: Insights into multi-stage Sn-polymetallic mineralization in South China. *Lithos* 312–313, 1–20. doi:10.1016/j.lithos.2018.05.001

Li, X. H., Li, W. X., Li, Z. X., Lo, C. H., Wang, J., Ye, M. F., et al. (2009). Amalgamation between the Yangtze and cathaysia blocks in South China: Constraints from SHRIMP U-Pb zircon ages, geochemistry and Nd-Hf isotopes of the Shuangxiwu volcanic rocks. *Precambrian Res.* 174 (1-2), 117–128. doi:10.1016/j.precamres.2009.07.004

Li, Z. X., Li, X. H., Wartho, J. A., Clark, C., Li, W. X., Zhang, C. L., et al. (2010). Magmatic and metamorphic events during the early Paleozoic Wuyi-Yunkai orogeny, southeastern South China: New age constraints and pressure-temperature conditions. *GSA Bull.* 122 (5–6), 772–793. doi:10.1130/B30021.1

Lin, S. F., Xing, G. F., Davis, D. W., Yin, C. Q., Wu, M. L., Li, L. M., et al. (2018). Appalachian-style multi-terrane Wilson cycle model for the assembly of South China. *Geology* 46 (4), 319–322. doi:10.1130/G39806.1

Liu, Y. S., Gao, S., Hu, Z. C., Gao, C. G., Zong, K. Q., and Wang, D. B. (2010). Continental and oceanic crust recycling-induced melt–peridotite interactions in the trans-north China orogen: U–Pb dating, Hf isotopes andtrace elements in zircons from mantle xenoliths. *J. Pet.* 51, 537–571. doi:10.1093/petrology/egp082

Loiselle, M. C., and Wones, D. (1979). Characteristics and origin of anorogenic granites. *Geol. Soc. Am. Abstr. Programs* 11, 468.

Ludwig, K. R. (2003). *User's manual for Isoplot 3.00: A geochronological toolkit for microsoft excel*. Berkeley, California: Special Publication 4aBerkeley Geochronology Center.

McCurry, M., Hayden, K. P., Morse, L. H., and Mertzman, S. (2008). Genesis of post-hotspot, A-type rhyolite of the Eastern Snake River Plain volcanic field by extreme fractional crystallization of olivine tholeiite. *Bull. Volcanol.* 79, 361–383. doi:10.1007/s00445-007-0143-4

Patiño Douce, A. (1997). Generation of metaluminous A-type granites by low-pressure melting of calc-alkaline granitoids. *Geology* 25, 743–746. doi:10.1130/0091-7613(1997)025<0743:gomatg>2.3.co;2

Peng, S. B., Jin, Z. M., Fu, J. M., Liu, Y. H., He, L. Q., and Cai, M. H. (2006). Geochemical characteristics of basic intrusive rocks in the Yunkai uplift, Guangdong-Guangxi, China, and their tectonic significance. *Geol. Bull. Chin.* 25, 434–441. doi:10.3969/j.issn.1671-2552.2006.04.002

Peng, S. B., Liu, S. F., Lin, M. S., Wu, C. F., and Han, Q. S. (2016). Early Paleozoic subduction in Cathaysia (II): New evidence from Dashuang high magnesian-magnesian andesite. *Earth Sci.* 41 (6), 931–947. doi:10.3799/dqkx.2016.079

Philpotts, A. R. (1990). *Principle of igneous and metamorphic Petrology*. New Jersey: Prentice-Hall, 498.

Ren, J. S., Niu, B. G., and Zheng, J. (1997). Tectonic frame and geodynamic evolution of eastern China. *Gondwana Res.* 29 (30), 43–55.

Schiller, D., and Finger, F. (2019). Application of Ti-in-zircon thermometry to granite studies: Problems and possible solutions. *Contrib. Mineral. Pet.* 174 (6), 51–16. doi:10.1007/s00410-019-1585-3

Shu, L. S., Jahn, B. M., Charvet, J., Santosh, M., Wang, B., Xu, X. S., et al. (2014). Early Paleozoic depositional environment and intraplate tectono-magmatism in the Cathaysia Block (South China): Evidence from stratigraphic, structural, geochemical and geochronological investigations. *Am. J. Sci.* 314 (1), 154–186. doi:10.2475/01.2014.05

Shu, L. S., Yu, J. H., Jia, D., Wang, B., Shen, W. Z., and Zhang, Y. Q. (2008). Early Paleozoic orogenic belt in the eastern segment of South China [in Chinese with English abstract]. *Geol. Bull. China.* 27 (10), 1581–1593. doi:10.3969/j.issn.1671-2552.2008.10.001

Shu, X. J., Gao, T. S., Zhou, X. H., and Li, H. L. (2020). A new report of the early Palaeozoic hornblendite in South China and its tectonic significance. *Geol. J.* 55 (1), 210–222. doi:10.1002/gj.3404

Shu, X. J., Liao, S. B., Tang, M., Hong, W. T., and Li, J. Y. (2021). Different water contents lead to contrasting magmatic differentiation pathways: A case study of two coeval rock suites. *Lithos* 386, 106000. doi:10.1016/j.lithos.2021.106000

Shu, X. J., Wang, X. L., Sun, T., Xu, X., and Dai, M. N. (2011). Trace elements, U–Pb ages and Hf isotopes of zircons from Mesozoic granites in the Western Nanling Range, South China: Implications for petrogenesis and W–Sn mineralization. *Lithos* 127 (3–4), 468–482. doi:10.1016/j.lithos.2011.09.019

Skjerlie, K. P., and Johnston, A. D. (1993). Fluid-absent melting behavior of an F-rich tonalitic gneiss at mid-crustal pressures: Implications for the generation of anorogenic granites. *J. Pet.* 34, 785–815. doi:10.1093/petrology/34.4.785

Sun, S. S., and McDonough, W. F. (1989). Chemical and isotopic systematics of oceanic basalts: Implications for mantle composition and processes. *Geo Soc. Lond. Spec. Pub* 42 (1), 313–345. doi:10.1144/gsl.sp.1989.042.01.19

Tong, L., Li, C., Liu, Z., Zhai, M., and Li, W. (2021). First report of phengites in the longyou paragneiss in the northern early paleozoic wuyi-yunkai orogen, South China: PT conditions, zircon U-Pb ages and tectonic implications. *J. Asian Earth Sci.* 214, 104754. doi:10.1016/j.jseaes.2021.104754

Vervoort, J. D., Patchett, P. J., Blichert–Toft, J., and Albarède, F. (1999). Relationships between Lu–Hf and Sm-Nd isotopic systems in the global sedimentary system. *Earth Planet. Sci. Lett.* 168, 79–99. doi:10.1016/s0012-821x(99)00047-3

Wang, Y. J., He, H. Y., Gan, C. S., and Zhang, Y. Z. (2018). Petrogenesis of the early silurian dashuang high-Mg basalt–andesite–dacite in eastern South China: Origin from a palaeosubduction-modified mantle. *J. Geol. Soc. Lond.* 175 (6), 949–966. doi:10.1144/jgs2018-102

Wang, Y. J., Zhang, A. M., Fan, W. M., Zhang, Y. H., and Zhang, Y. Z. (2013). Origin of paleosubduction-modified mantle for Silurian gabbro in the Cathaysia Block: Geochronological and geochemical evidence. *Lithos* 160-161, 37–54. doi:10.1016/j.lithos.2012.11.004

Watson, E. B., and Harrison, T. M. (2005). Zircon thermometer reveals minimum melting conditions on earliest Earth. *Science* 308 (5723), 841–844. doi:10.1126/science.1110873

Xia, Y., Xu, X. S., Zou, H. B., and Liu, L. (2014). Early paleozoic crust–mantle interaction and lithosphere delamination in SouthSouth China block: Evidence from geochronology, geochemistry, and Sr–Nd–Hf isotopes of granites. *Lithos* 184, 416–435. doi:10.1016/j.lithos.2013.11.014

Xin, Y. J., Li, J. H., Ratschbacher, L., Zhao, G. C., Zhang, Y. Q., Dong, S. W., et al. (2020). Early devonian (415–400 Ma) A-type granitoids and diabases in the wuyishan, eastern cathaysia: A signal of crustal extension coeval with the separation of SouthSouth China from gondwana. *GSA Bull.* 132 (11–12), 2295–2317. doi:10.1130/b35412.1

Xu, W. J., and Xu, X. S. (2017). An early paleozoic monzonorite-granite suite in the SouthSouth China block: Implications for the intracontinental felsic magmatism. *Mineral. Pet.* 111 (5), 709–728. doi:10.1007/s00710-016-0488-5

Xu, W. J., and Xu, X. S. (2015). Early paleozoic intracontinental felsic magmatism in the SouthSouth China block: Petrogenesis and geodynamics. *Lithos* 234–235, 79–92. doi:10.1016/j.lithos.2015.08.006

Xu, X. S., O'Reilly, S. Y., Griffin, W. L., Wang, X., Pearson, N. J., and He, Z. Y. (2007). The crust of cathaysia: Age, assembly and reworking of two terranes. *Precambrian Res.* 158 (1-2), 51–78. doi:10.1016/j.precamres.2007.04.010

Yao, J. L., Cawood, P. A., Shu, L. S., and Zhao, G. C. (2019). Jiangnan orogen, South China: a~ 970–820 Ma rodinia margin accretionary belt. *Earth-Sci. Rev.* 196, 102872. doi:10.1016/j.earscirev.2019.05.016

Yao, W. H., Li, Z. X., Li, W. X., Wang, X. C., Li, X. H., and Yang, J. H. (2012). Post-kinematic lithospheric delamination of the Wuyi–Yunkai orogen in South China: Evidence from ca. 435 Ma high-Mg basalts. *Lithos* 154, 115–129. doi:10.1016/j.lithos.2012.06.033

Yi, L. W., Ma, C. Q., Wang, L. X., Lai, Z. X., Li, X. Y., Yang, Y. N., et al. (2014). Discovery of late ordovician subvolcanic rocks in SouthSouth China: Existence of subduction-related dacite from early paleozoic. *Earth Sci.—J. Chin. Uni. Geosci.* 39 (6), 637–653. doi:10.3799/dqkx.2014.061

Yu, J. H., Lou, F. S., Wang, L. J., Shen, L. W., Zhou, X. Y., Zhang, C. H., et al. (2014). The geological significance of a Paleozoic mafic granulite found in the Yiyang area of northeastern Jiangxi Province. *Chin. Sci. Bull.* 59 (35), 3508–3516. doi:10.1360/n972014-00395

Yu, J. H., Zhou, X. M., O'Reilly, Y. S., Zhao, L., Griffin, W. L., Wang, R. C., et al. (2005). Formation history and protolith characteristics of granulite facies metamorphic rock in Central Cathaysia deduced from U-Pb and Lu-Hf isotopic studies of single zircon grains. *Chin. Sci. Bull.* 50 (18), 2080–2089. doi:10.1360/982004-808

Zhang, C. L., Zhu, Q. B., Chen, X. Y., and Ye, H. M. (2016). Ordovician arc related mafic intrusions in South China: Implications for plate subduction along the southeastern margin of South China in the early Paleozoic. *J. Geol.* 124 (6), 743–767. doi:10.1086/688640

Zhang, F. R., Shu, L. S., Wang, D. Z., Shen, W. Z., Yu, J. H., and Xie, L. (2010). Study on geochronological, geochemical features and Genesis of the fufang granitic pluton in the Jiangxi Province, South China. *Geol. J. China Univ.* 16 (2), 161–176. doi:10.16108/j.issn1006-7493.2010.02.003

Zhang, Q., Jiang, Y. H., Wang, G. C., Liu, Z., Ni, C. Y., and Qing, L. (2015). Origin of Silurian gabbros and I-type granites in central Fujian, SE China: Implications for the evolution of the early Paleozoic orogen of South China. *Lithos* 216–217, 285–297. doi:10.1016/j.lithos.2015.01.002

Zhao, J. H., Yang, T., and Wang, W. (2022). Orogenic belt resulting from ocean-continent collision. *Geology* 50, 1266–1269. doi:10.1130/g50337.1

Zhao, K. D., Jiang, S. Y., Sun, T., Chen, W. F., Ling, H. F., and Chen, P. R. (2013). Zircon U-Pb dating, trace element and Sr-Nd-Hf isotope geochemistry of paleozoic granites in the miao'ershan-yuechengling batholith, South China: Implication for petrogenesis and tectonic-magmatic evolution. *J. Asian Earth Sci.* 74, 244–264. doi:10.1016/j.jseaes.2012.12.026